

Automatic Boundary Evolution Tracking via a Combined Level Set Method and Mesh Warping Technique: Application to Hydrocephalus^{*}

Jeonghyung Park¹, Suzanne M. Shontz², and Corina S. Drapaca¹

¹ The Pennsylvania State University, University Park, PA 16802, USA

² Mississippi State University, Mississippi State, MS 39762, USA
jxp975@cse.psu.edu, sshontz@math.msstate.edu, csd12@psu.edu

Abstract. Hydrocephalus is a neurological disease which causes ventricular dilation due to abnormalities in the cerebrospinal fluid (CSF) circulation. Although treatment via a CSF shunt in the brain ventricles has been performed, poor rates of patient responses continue. Thus, to aid surgeons in hydrocephalus treatment planning, we propose a geometric computational approach for tracking hydrocephalus ventricular boundary evolution via the level set method and a mesh warping technique. In our previous work [1], we evolved the ventricular boundary in 2D CT images which required a backtracking line search for obtaining valid intermediate meshes. In this paper, we automatically detect the ventricular boundary evolution for 2D CT images. To help surgeons determine where to implant the shunt, we also compute the brain ventricle volume evolution for 3D MR images using our approach.

1 Introduction

Hydrocephalus is a neurological disease characterized by abnormalities in the cerebrospinal fluid (CSF) circulation, resulting in ventricular dilation. The CSF is formed within the cerebral ventricles by the choroid plexuses and the brain parenchyma, circulates through the ventricles and within the subarachnoid space surrounding the brain, and drains into the venous blood by passing through the arachnoid villi located in the dura matter [18]. Currently, it is believed that hydrocephalus may be caused by increased CSF production, by obstruction of CSF circulation or of the venous outflow system, or due to genetic factors. The efforts in treatment have been principally through CSF flow diversion. Within limits, the dilation of the ventricles can be reversed by either CSF shunt implantation or by performing an endoscopic third ventriculostomy (ETV) surgery, resulting in a relief from the symptoms of hydrocephalus. However, despite the technical advances in shunt technology and endoscopy, the two treatments show no statistically significant difference in the efficacy for treating hydrocephalus

^{*} The work of the first author was funded by NSF CAREER Award OCI-1054459; the work of the second author was funded in part by NSF CAREER Award OCI-1054459 and NSF grant CNS-0720749.

[24]. ETV performs well only in some clinical cases of hydrocephalus [13], whereas shunt failure happens in over 60% of patients [16]. There is therefore an urgent need to design better therapy protocols for hydrocephalus.

An important step in this direction is the development of predictive theoretical and computational models of the mechanics of hydrocephalus. The Monroe-Kellie hypothesis [17, 20] reduces the dynamics of the cranium to a competition for space among CSF, blood, and brain parenchyma. This idea leads to numerous pressure-volume models [22] (and references within) where the CSF is contained within one compartment surrounded by compliant walls representing the brain parenchyma. However, these models provide little insight towards a more fundamental understanding of the mechanisms of hydrocephalus. In [15], Hakim proposed to model the brain parenchyma as a porous sponge of viscoelastic material. Nagashima [21] extended this model by applying Biot's theory of consolidation and carried out finite element simulations of the resulting mathematical model. This introduced one of the two current models of brain biomechanics, namely the poroelastic model [23, 25], in which the brain is a porous linearly elastic sponge saturated in a viscous incompressible fluid. The second modeling approach considers the brain parenchyma to be a linear viscoelastic material [19, 26]. Unlike the linear viscoelastic and poroelastic models which are based on the assumption of small strain theory, the quasi-linear viscoelastic model proposed in [14] was the first to successfully predict the large ventricular displacements in hydrocephalus. Most of the above-mentioned mechanical models, however, use either a cylindrical or a spherical geometry for the brain.

In order for mechanical models of brain to be of clinical relevance their corresponding computational algorithms and software must incorporate the structural geometry of the brain as seen in medical images as well as efficient and robust numerical solvers. In our recent work [1, 12], we used nonlinear constitutive laws and two-dimensional medical images of brains to simulate the response of hydrocephalic brains to treatments. In this paper, we generalize the results from [1] and propose an automatic computational pipeline for the evolution of the brain ventricles that involves the following steps: image denoising, threshold-based image segmentation, prediction of the ventricular boundaries via the level set method, generation of computational meshes of the brain, mesh deformation based using the finite element-based mesh warping (FEMWARP) method, and mesh quality improvement of the deformed meshes. We will present three-dimensional changes in the geometry of the lateral ventricles of a normal brain during simulated development of hydrocephalus, in the particular case when hydrocephalus is due to the occlusion of the interventricular foramina. The interventricular foramina (or foramina of Monro) are channels that connect the lateral ventricles with the third ventricle of the brain, and allow the CSF produced in the lateral ventricles to flow into the third ventricle and then to the rest of the brain.

2 Computational Techniques for Motion of Geometric Models and Meshes in Biomedical Simulations

Level-set methods (LSM) (e.g., [9, 27–30]) are computational techniques for tracking evolving curves or surfaces and have been used extensively in medical imaging and in other fields. The level set approach delineates region boundaries using closed parametric curves (or surfaces, etc.) that deform according to motion prescribed by a partial differential equation (PDE). The problem of how to move the curves is formulated as a front evolution problem. The final contour position is influenced by the speed of the deformation, which may be controlled by local curvature of the contour, the intensity gradient in an image, shape, the initial position of the contour [9], and the intrinsic physics of the problem. One important advantage of LSM is that deforming shapes undergoing topological changes can easily be tracked. This makes the LSM ideal for tracking the evolution of hydrocephalic brain ventricles.

Persson *et al.* developed a moving mesh technique [31, 32] for image-based problems which is based on the incorporation of level sets into an adaptive mesh refinement technique which uses a Cartesian or octree background mesh to determine the mesh motion. Alternatively, mesh warping algorithms compute the mesh deformation from the source domain to the target domain based upon interpolation and/or extrapolation of the vertex coordinates. Several mesh warping techniques for biomedical applications have been developed (e.g., [33–36]). However, none of these techniques were designed to handle the large deformations the ventricles undergo due to hydrocephalus.

3 Introduction to the Level Set Method and FEMWARP

In this section, we describe the particular level set and mesh warping methods we employ in our geometric computational pipeline.

3.1 The Chan and Vese Level Set Method for Curve Evolution

The Chan and Vese method [37] evolves level set curves using minimization of an energy functional of Mumford-Shah type.

Let u_0 denote a given image with domain Ω and C denote a parametrized curve. Let ϕ be a Lipschitz function which implicitly represents C . The zero-level curve of the function at time t of the function $\phi(t, x, y)$ is used to evolve C based on a prescribed speed and direction.

Let c_1 and c_2 be constants depending on C which are the averages of u_0 inside and outside of C , respectively, and let $F(c_1, c_2, \phi)$ denote the energy functional to be minimized by computing the Euler-Lagrange equations and then solving the resulting PDE. Let $\mu \geq 0, \nu \geq 0, \lambda_1$, and λ_2 be fixed parameters, and let $H_\epsilon, \delta_\epsilon$ be regularized Heaviside functions and one-dimensional Dirac measures, respectively. The curve evolution is obtained by minimizing the following

regularized energy functional:

$$\begin{aligned}
F_\epsilon(c_1, c_2, \phi) = & \mu \int_\Omega \delta_\epsilon(\phi(x, y)) |\nabla \phi(x, y)| \, dx \, dy \\
& + \nu \int_\Omega H_\epsilon(\phi(x, y)) \, dx \, dy \\
& + \lambda_1 \int_\Omega |u_0(x, y) - c_1|^2 H_\epsilon(\phi(x, y)) \, dx \, dy \\
& + \lambda_2 \int_\Omega |u_0(x, y) - c_2|^2 (1 - H_\epsilon(\phi(x, y))) \, dx \, dy.
\end{aligned} \tag{1}$$

The Chan and Vese technique is also known as the active contours without edges method, since the stopping criteria does not depend on the gradient of the image but rather on a particular segmentation of the image in which the given image is approximated by a piecewise constant function. We solve the energy minimization problem for (1) using the Matlab implementation by Wu in [40].

3.2 The Shontz and Vavasis Finite Element-Based Mesh Warping (FEMWARP) Algorithm

FEMWARP is a topology-preserving, tetrahedral mesh warping approach which was proposed by Baker [38] and was developed by Shontz and Vavasis [39].

First, FEMWARP represents each interior vertex in the mesh as a specific linear combination of its neighbors by computing the global stiffness matrix A for the boundary value problem $\Delta u = 0$ on Ω with $u = u_0$ on $\partial\Omega$ is formed, where Ω is the mesh domain, and A is computed based on piecewise linear finite elements on the mesh. Because only A is kept, any u_0 may be prescribed.

Let x be a vector containing the x -coordinates of the initial mesh vertices (and similarly for the y and z coordinates). It follows that

$$A_I[x_I, y_I, z_I] = -A_B[x_B, y_B, z_B], \tag{2}$$

where A_I and A_B are the submatrices of A with the rows indexed by interior vertices and the columns indexed by interior and boundary vertices, respectively.

Second, FEMWARP solves the above linear system, i.e., (2) with a new right-hand side vector based on the new boundary vertex positions (i.e., $[\hat{x}_B, \hat{y}_B, \hat{z}_B]$) (established by the level set method in our case) for the new coordinates of the interior vertices of the deformed mesh. In particular, we solve (3)

$$A_I[\hat{x}_I, \hat{y}_I, \hat{z}_I] = -A_B[\hat{x}_B, \hat{y}_B, \hat{z}_B] \tag{3}$$

for $[\hat{x}_I, \hat{y}_I, \hat{z}_I]$.

4 Ventricular Boundary Deformation with the Level Set Method and FEMWARP for Hydrocephalus Treatment

To track the evolution of the brain ventricles during treatment of hydrocephalus, we propose a combined level set/mesh warping algorithm. Our approach is designed as a computational pipeline and includes the following steps: image denoising, image segmentation, obtaining boundary vertices via the LSM, mesh

Algorithm 1 Mesh warping with the level set method

```

1: Input: medical images with source and target ventricular boundaries
2: Image denoising using mask filters
3: Image segmentation via thresholding method
4: Obtain ventricular boundary vertices from segmented source and target medical images via level set method
5: Generate initial mesh with A using Triangle
6: LOOP 1: Deform mesh from source to target using FEMWARP
7: if mesh is valid then
8:   Mesh quality improvement on the deformed mesh
9:   return mesh
10: else
11:   Backtracking line search with small-step FEMWARP until mesh is valid
12: end if
13: Go to LOOP 1

```

generation, LSM and mesh warping, and mesh quality improvement. Pseudocode for our combined level set/mesh warping algorithm is given in Algorithm 1. More details for each step of the algorithm are given in [1].

We performed two simulations based on our combined level set/mesh warping algorithm shown in Algorithm 1. The first simulation was ventricular boundary deformation for 2D CT images via the LSM. Unlike our previous study [1], the evolution of the ventricular boundary was automatically detected via the LSM in the first simulation. The second simulation was the ventricular boundary evolution of 3D brain images. The motion of the 3D brain ventricles was simulated based on the LSM with a constant speed movement. The Solaris machine employed for the simulations was an UltraSPARC-III CPU with a 750MHz processor, 1GB SDRAM of memory, and an 8MB L2 cache.

4.1 Simulation 1: Automatic Boundary Detection via Level Set Method

Three CT images [2], i.e., pre-treatment, period 1 (6 months later), and period 2 (1 year later) of hydrocephalus treatment via shunt insertion, are used as inputs for this simulation. In our previous study, the LSM was applied only to obtain the ventricular boundary vertices in the segmented images. The intermediate boundary deformation from pre-treatment to period 1 and from period 1 to period 2 was determined by using a backtracking line search.

In this simulation, however, the intermediate boundary vertices were obtained by applying the LSM instead of using a backtracking line search. When detecting the boundary vertices in an image, the LSM sets up an initial boundary contour starting as a zero curve. This initial contour moves toward the ventricular boundary in the image based on the movement computed by the LSM.

In each iteration, the LSM moves the initial contour toward the next target boundary. The contours of each iteration represent the deformation of the brain

ventricles. Thus, by tracking the boundary movement via the LSM, the intermediate boundary vertices for the deformation are obtained. Since the variation of the boundary movement between intermediate steps is very small, the automatic intermediate boundary detection steps generate valid meshes and use of a backtracking line search is not required.

Image denoising was performed as the first step of the simulation. For the pre-treatment, period 1 and period 2 CT images, 3×3 , 6×6 , and 4×4 mask filters were applied [8]. When segmenting the denoised images, threshold-based segmentation method was performed [7] with threshold values of 20, 77, and 45 for the pre-treatment, period 1, and period 2 images. After segmentation, the ventricles in the segmented images were represented as zero-valued pixels, and the remaining parts were represented as one-valued pixels.

From the segmented pre-treatment image, the LSM was applied to obtain the boundary vertices of the ventricles in the image. The contour for the zero function obtained by the LSM matched the boundary of the ventricles in the segmented pre-treatment image. The ventricular boundary obtained from the segmented pre-treatment image was used as an initial contour of the LSM for boundary detection of the segmented period 1 image. For each ventricular boundary vertex, the next vertex is selected from the boundary vertices a fixed Euclidean distance from the given vertex. The coordinates of the boundary vertices are computed and ordered by repeating this process. The LSM moved the contour in the inward normal direction with a constant speed of $13.2e^{-12}$ to detect the boundary of the ventricles in the segmented period 1 image. Since the movement was slow, all intermediate steps computed by the LSM generated valid meshes. The level set method evolved until the average of the absolute distance between the previous and the current contour vertices was smaller than 10^{-9} .

Similar to the process of obtaining the boundary of the ventricles in the segmented period 1 image, the ventricular boundary of the segmented period 2 image was obtained. The ventricular boundary of the segmented period 1 image was used as an initial contour of the LSM to obtain the ventricular boundary of the segmented period 2 image.

An initial mesh for the segmented pre-treatment image was generated using Triangle [3]. By using the boundary vertices obtained automatically from the LSM, mesh deformation for the ventricles was performed. Mesh deformation with intermediate steps from pre-treatment to period 1, and from period 1 to period 2 was performed by FEMWARP algorithm [39].

Figure 1 shows initial, intermediate, and final meshes generated during ventricular mesh deformation via the LSM with automatic intermediate boundary detection. The boundary deformation in the figure was obtained in reverse (i.e., from the period 2 segmented image to the pre-treatment image). Since the LSM detects expanding boundaries better than shrinking ones, the intermediate boundaries were easily obtained and valid meshes were generated without the use of a backtracking line search. After each intermediate mesh deformation step, average mesh quality improvement was performed by feasible Newton

method [5] in Mesquite [4]. The inverse mean ratio [5] mesh quality distribution for the intermediate meshes are shown in Figure 2.

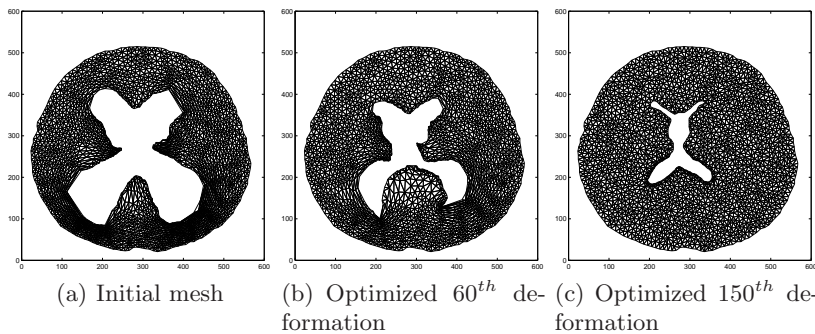


Fig. 1. (a) The mesh having the ventricular boundary vertices matched to pre-treatment ventricular boundary vertices. The mesh contained 2187 vertices and 4026 elements. ((b) and (c)) the deformed meshes generated by the FEMWARP algorithm [39]. The 60th and 150th intermediate mesh deformation results matched exactly to the boundary vertices for the ventricles in the segmented period 1 and period 2 images. Mesh quality improvement was performed to improve the mesh quality at each step of the hydrocephalus ventricular deformation.

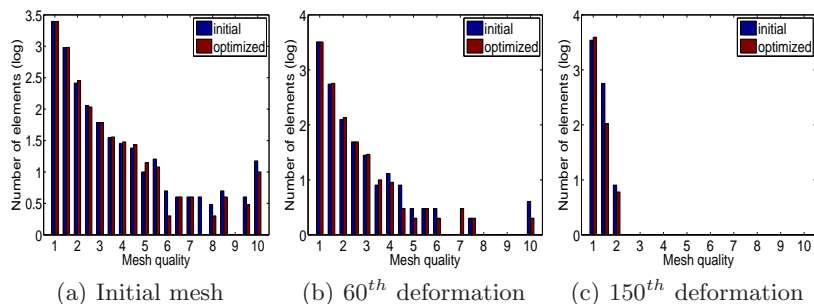


Fig. 2. Inverse mean ratio mesh quality distribution for meshes generated in Simulation 1. Quality distribution for (a) the initial mesh, (b) the 60th deformation, and (c) the 150th deformation.

4.2 Simulation 2: 3D Ventricular Mesh Deformation via Level Set Method and FEMWARP

We obtained a 3D MR image of the normal brain containing 181 2D brain MRI slices from [6]. The goal of this experiment was to simulate 3D ventricular

deformation from the normal to hydrocephalic state. In this simulation, the intermediate boundaries were computed by expanding the volume of the normal brain ventricles using LSM [9], as no target image is available in this dataset. The boundary of the expanded ventricles was used as an intermediate boundary of ventricular deformation. If a target MR image were available, our approach could also be used to simulate hydrocephalus treatment.

In order to obtain the brain ventricle volume, the 3D brain is created by segmenting the 3D MRI. First, all 181 2D MR images were denoised using a 3×3 mask filter [8]. After image denoising was performed, the images were segmented based on threshold value of 50 [7]. In each segmented image, the white parts represent the brain tissue, and the black parts represent the brain ventricles, which will be deformed via the LSM. The segmented 2D images were stacked on top of each other to create a segmented 3D MRI [10]. By extracting the portion of the image represented as voxels with a value of zero in the reconstructed 3D MR image, the brain ventricle volume was obtained and is shown in Figure 3(a).

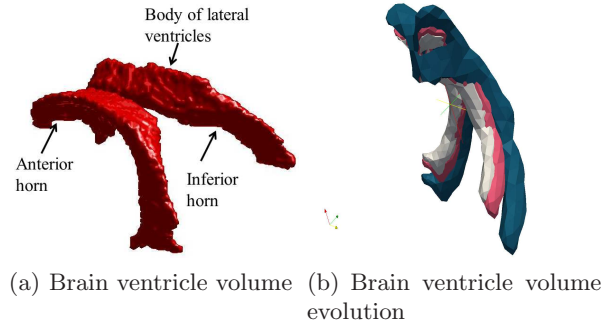


Fig. 3. (a) The brain ventricle volume obtained from the segmented 3D MR image. (b) The brain ventricle volume evolution via the LSM [9].

To obtain the boundary vertices of the volumetric brain ventricles, the Matlab function isosurface was used. With the boundary vertex information, the initial mesh for the 3D brain MR image was generated by Tetgen [11]. After obtaining the ventricular boundary vertices, the ventricular boundary deformation was computed via the LSM. The boundary obtained from the segmented 3D MR image was used as an input zero surface of the LSM. To evolve the ventricular boundary, the LSM [9] moved the boundary of the 3D ventricles along their interior normals with a constant speed of 0.01. Once the ventricular boundary surface was evolved, the normals of the previous boundary vertices were computed. The next position of each boundary vertex was computed by selecting the point where the normal meets the evolved surface. In this simulation, the ventricular boundary evolution was terminated after 10 iterations since the expanded ventricle brain volume was similar to the hydrocephalic state. The evolved brain ventricular volumes are shown in Figure 3(b).

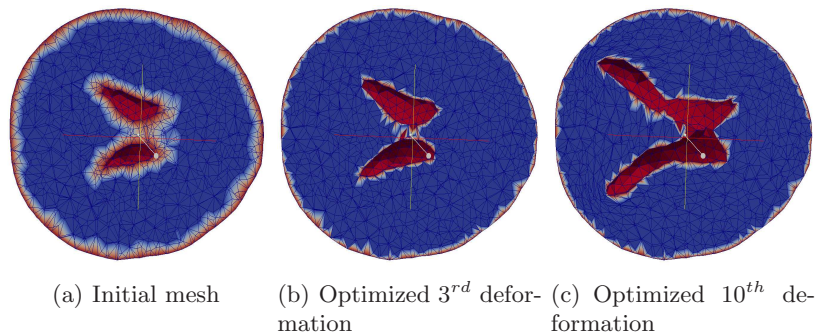


Fig. 4. (a) The mesh having the ventricular boundary vertices matched to the 3D normal brain MRI. ((b) and (c)) the deformed meshes generated by the FEMWARP algorithm [39]. Each evolved surface was computed via the 3D LSM with constant speed of 0.01. The mesh contained 8200 vertices and 40,783 elements. The blue-colored brain represents the part to be deformed. Mesh quality improvement was performed to improve the mesh quality at each step of the brain ventricular volume deformation.

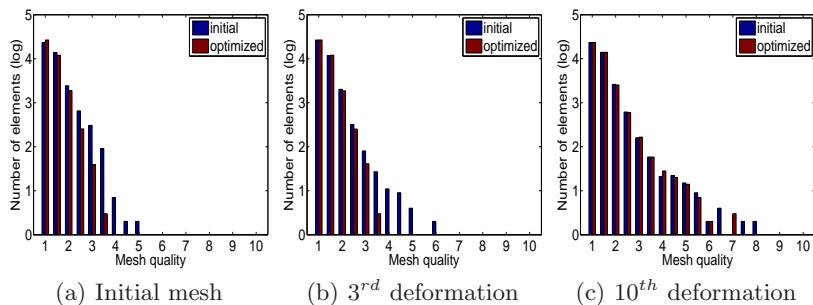


Fig. 5. Inverse mean ratio mesh quality distribution for meshes generated in Simulation 2. Quality distribution for (a) the initial mesh, (b) the 3rd deformation, and (c) the 10th deformation.

When computing the new contour position, the mesh was deformed via FEMWARP [39]. Also, mesh quality improvement for the intermediate step was performed once the deformed mesh was obtained. The optimized mesh was used as input in the computation of the next intermediate deformation step. Figure 4 shows the initial, intermediate, and final meshes obtained during 3D brain ventricle boundary deformation. In each iteration, the mesh deformed by FEMWARP [39] was valid; hence, a backtracking line search was not required. Feasible Newton [5] mesh quality improvement via Mesquite [4] was performed after each boundary deformation step. The brain ventricle volume was expanded three times bigger than its initial volume. Figure 5 shows the inverse mean ratio [5] mesh quality distribution for the intermediate meshes. Unlike the previous simulation, since the brain ventricle volume was enlarging to establish hydrocephalus, the mesh parts to be deformed and analyzed shrunk. Thus, the mesh

quality distribution for the 10th iteration is worse than that of the previous iterations. In spite of this, the mesh quality was constantly monitored to ensure the mesh quality was good enough for simulation.

5 Conclusions

In our previous research [1], we develop an image-based ventricular evolution tracking method via the LSM [9] and FEMWARP [39]. In this paper, we proposed two new techniques: the automatic ventricular boundary deformation for 2D CT images and the brain ventricle volume deformation for 3D MR image via the LSM and FEMWARP. This approach can be used for any types of medical images such as CT, MR, and ultrasound. Compared to our previous work [1], the ventricular boundary deformation for 2D CT images was computed automatically via the LSM. There were no invalid meshes in deformed meshes generated by the automatic boundary detection process via the LSM. Thus, no backtracking line search was required. Simulation results showed that the 2D ventricular boundary deformation via FEMWARP with the ventricular boundaries obtained from the automatic LSM boundary detection was successfully performed.

Also, deformation of the brain ventricle volume for a 3D MRI was performed, which is an extension of our previous work [1]. Since no target MR images are available to us, a 3D normal brain MRI was used for computing the ventricle volume evolution for the simulation. To evolve the brain ventricle volume, the LSM computed the evolved boundaries. By using the evolved brain ventricle boundary, the brain ventricle volume deformation was performed via FEMWARP successfully. Unlike our previous work, no actual topological changes occurred when 3D brain ventricular volume deformation was performed. Through our approach, we aid neurosurgeons in easily determining where to place the shunt and thus in obtaining better prognosis of hydrocephalus treatment. We will extend our geometric computational approach to incorporate the mechanics of hydrocephalus. We will also apply our technique to patient 3D MRIs.

References

1. Park, J., Shontz, S., Drapaca, C.: A combined level set/mesh warping algorithm for tracking brain and cerebrospinal fluid evolution in hydrocephalic patients, *Image-based Geometric Modeling and Mesh Generation. Lecture Notes in Computational Vision and Biomechanics*, Springer, Editor: Zhang, J. (To appear, 2012).
2. West, J.: Application of the level set method to hydrocephalus: Simulating the motion of the ventricles. Master's thesis, University of Waterloo (2004).
3. Shewchuk, J.: Triangle: Engineering a 2D quality mesh generator and delaunay triangulation. In: *Applied Computational Geometry: Towards Geometric Engineering*, vol.1148, 203–222, Springer-Berlin Lecture Notes in Computer Science (1996).
4. Brewer, M., Diachin, L., Knupp, P., Leurent, T., Melander, D.: The Mesquite mesh quality improvement toolkit. In: *Proc. of the 12th International Meshing Roundtable*, 239–250, Sandia National Laboratories (2003).

5. Munson, T.: Mesh shape-quality optimization using the inverse mean-ratio metric, *Math. Program* 110, 561–590, (2007).
6. Cocosco, C.A., Kollokian, V., Kwan, R.K.-S., Evans, A.C.: BrainWeb: Online interface to a 3D MRI simulated brain database, *NeuroImage*, In: Proc. of 3rd International Conference on Functional Mapping of the Human Brain, vol.5, no.4, part 2/4, S425, (1997).
7. Zhu, S., Xia, X., Zhang, Q., Belloulata, K.: An image segmentation algorithm in image processing based on threshold segmentation, In: Proc. of the 2007 Third International IEEE Conference on Signal-Image Technologies and Internet-Based System, 673–678, (2007).
8. Fabijanska, A.: Variance filter for edge detection and edge-based image segmentation, In: Proc. of 7th International Conference on Perspective Technologies and Methods in MEMS Design, 151–154, (2011).
9. Sethian, J.: *Level Set Methods and Fast Marching Methods: Evolving Interfaces in Computational Geometry, Fluid Mechanics, Computer Vision, and Materials Science*, Cambridge Monographs on Applied and Computational Mathematics (1999).
10. Narayanan, K., Karunakar, Y.: 3-D reconstruction of tumors in MRIs, *International Journal of Research and Reviews in Signal Acquisition and Processing*, Vol.1, no.2, (2011).
11. Si, H.: *TetGen: A Quality Tetrahedral Mesh Generator and 3D Delaunay Triangulator Version 1.4*, (2006).
12. Roy, S., Heltai, L., Drapaca, C.S., Costanzo, F.: An immersed finite element method approach for brain Biomechanics, to appear in the Proc. of SEM, (2012).
13. Choi, J.U., Kim, D.S., Kim, S.H.: Endoscopic surgery for obstructive hydrocephalus, *Yonsei Med. J.* 40(6):600-607, (1999).
14. Drapaca, C.S., Tenti, G., Rohlf, K., Sivaloganathan, S.: A quasi-linear viscoelastic constitutive equation for the brain: Application to hydrocephalus, *J. Elasticity* 85:65-83, (2006).
15. Hakim, S., Venegas, J., Burton, J.: The physics of the cranial cavity, hydrocephalus and normal pressure hydrocephalus: Mechanical interpretation and mathematical model, *Surg. Neurol.* 5:187-210, (1976).
16. Hydrocephalus statistics. See <http://www.ghrforg.org/faq.htm>, (2008).
17. Kellie, G.: Appearances observed in the dissection of two individuals; death from cold and congestion of the brain, *Trans. Med-Chir. Soc. Edinburgh* 1-84, (1824).
18. Milhorat, T. H. *Pediatric Neurosurgery*. Contemporary Neurology Series:16, (1978).
19. Miller, K., Chinzei, K.: Constitutive modeling of brain tissue - experiment and theory, *J. Biomech.* 30:1115-1121, (1997).
20. Monro, A.: *Observations on Structure and Functions of the Nervous System*, Edinburgh: Creech and Johnson, (1783).
21. Nagashima, T., Tamaki, N., Matsumoto, S. Horwitz, B., Seguchi, Y.: Biomechanics of hydrocephalus: A new theoretical model, *Neurosurg* 21 (6):898-904, (1987).
22. Sivaloganathan, S., Tenti, G., Drake, J.: Mathematical pressure volume models of the cerebrospinal fluid, *Appl. Math. Comput.* 94:243-266, (1998)
23. Tenti, G., Sivaloganathan, S., Drake, J.: Brain biomechanics: steady-state consolidation theory of hydrocephalus, *Can. App. Math. Q.* 7 (1):111-124, (1999).

24. Tuli, S., Alshail, E., Drake, J.: Third ventriculostomy versus cerebrospinal fluid shunt as a first procedure in pediatric hydrocephalus, *Pediatr. Neurosurg.* 30(1):11-15, (1999).
25. Tully, B., Ventikos, Y.: Coupling poroelasticity and CFD for cerebrospinal fluid hydrodynamics, *IEEE Trans. Biomed. Eng.*, 56(6):1644–1651, (2009).
26. Wilkie, K., Drapaca, C.S. Sivaloganathan, S.: A theoretical study of the effect of ventricular pressure pulsations on the pathogenesis of hydrocephalus, submitted to *Appl. Math. Comput.* (2009).
27. Osher, S., Sethian, J.: Fronts propagating with curvature dependent speed: Algorithms based on Hamilton-Jacobi formulations. *J. Comput. Phys.* 79, 12–49 (1988).
28. Vese, L., Chan, T.: A multiphase level set framework for image segmentation using the Mumford and Shah model. *Int. J. Comput. Vision* 50, 271–293 (2002).
29. Osher, S., Fedkiw, R.: *Level Set Methods and Dynamic Implicit Surfaces*, Applied Mathematical Sciences vol. 153. Springer (2003).
30. Mitich, A., Ayed, I.: *Variational and level set methods in image segmentation*. Springer Topics in Signal Processing vol.5, Springer (2010).
31. Persson, P.: Mesh size functions for implicit geometries and PDE-based gradient limiting. *Engineering with Computers* 22, 95–109 (2006).
32. Strang, G., Persson, P.: Circuit simulation and moving mesh generation. In: *Proc. of Int. Symp. on Comm. and Inform. Tech. 2004 (ISCIT 2004)* (2004).
33. Bah, M., Nair, P., Browne, M.: Mesh morphing for finite element analysis of implant positioning in cementless total hip replacement. *Med. Eng. Phys.* 31, 1235–1243 (2009).
34. Baldwin, M., Langenderfer, J., Rullkoetter, P., Laz, P.: Development of subject-specific and statistical shape models of the knee using an efficient segmentation and mesh-morphing approach. *Comput. Meth. Prog. Bio.* 97, 232–240 (2010).
35. Liu, Y., D’Arceuil, H., He, J., Duggan, M., Gonzalez, G., Pryor, J., de Crespigny, A.: A nonlinear mesh-warping technique for correcting brain deformation after stroke. *Magn. Reson. Imaging* 24, 1069–1075 (2006).
36. Sigal, I., Yang, H., Roberts, M., Downs, J.: Morphing methods to parameterize specimen-specific finite element model geometries. *J. Biomech.* 43, 254–262 (2010).
37. Chan, T., Vese, L.: Active contours without edges. *IEEE T. Image. Process.* 10 (2001).
38. Baker, T.: Mesh movement and metamorphosis. In: *Proc. of the Tenth International Meshing Roundtable*, 387–396. Sandia National Laboratories (2001).
39. Shontz, S., Vavasis, S.: Analysis of and workarounds for element reversal for a finite elementbased algorithm for warping triangular and tetrahedral meshes. *BIT, Numerical Mathematics* 50, 863–884 (2010).
40. Wu, Y.: Matlab implementation of the Chan Vese active contour without edges method. (2011) See <http://www.mathworks.com/matlabcentral/fileexchange/23445>.